Assembly of Fully Substituted 2H-Indazoles Catalyzed by Cu₂O Rhombic Dodecahedra and Evaluation of Anticancer Activity

Rajeeva Lochana Panchangam,[a] Venkatraman Manickam,*[a] and Kaushik Chanda*[b]

Simultaneous C—N, and N—N bond-forming methods for one-pot transformations are highly challenging in synthetic organic chemistry. In this study, the Cu₂O rhombic dodecahedra-catalyzed synthesis of 2H-indazoles is demonstrated with good to excellent yields from readily available chemicals. This one-pot procedure involves Cu₂O nanoparticle-catalyzed consecutive C—N, and N—N bond formation followed by cyclization to yield 2H-indazoles with broad substrate scope and high functional group tolerance. Various cell-based bioassay studies demonstrated that 2H-indazoles inhibit the growth of cancer cells, typically through induction of apoptosis in a dose-dependent manner. Moreover, 2H-indazoles tested in the MDA-MB-468 cell line were capable of inhibiting cancer cell migration and invasion. Thus, it is shown that 2H-indazoles have potent in vitro anticancer activity that warrant further investigation of this compound class.

Introduction

Heterocyclic compounds obtained by diversity-oriented synthesis are widely found in natural products and bioactive molecules and have a vast array of applications across numerous fields.[1] Over the last decade, researchers in drug discovery have paid more attention to indazole derivatives, as this moiety acts as a bioisostere of indoles and benzimidazoles.[2] Molecules with 2H-indazole moieties have a wide range of biological properties, such as antitumor activity,[3] HIV-protease inhibition,[4] anti-inflammatory activity,[5] and modulation of estrogen receptors.[6] Moreover, in addition to these biological activities, indazole scaffolds also exhibit photophysical properties for potential theranostic applications.[7] The core 2H-indazole structure has been found in many drugs (Figure 1), such as niraparib (A), pazopanib (B), and a covalent inhibitor (C) that targets drug-resistant tumors over-expressing the epidermal growth factor receptor.[8] Moreover, related heterocycles have also been used in Ru-catalyzed C—H bond activation reactions.[9]

In view of their wide-ranging bioactivities, several synthetic methods have been developed for the synthesis of indazole moieties. However, to date, most attention has been directed toward the synthesis of thermodynamically stable 1H-indazoles as compared with their 2H-congeners.[10] Owing to the recently

discovered potent bioactivity of 2H-indazole moieties, several research groups have developed a number of synthetic strategies. The most common synthetic strategies involve the use of Pd-catalyzed domino reactions of 2-halophenyl acetylenes with hydrazines, [3 + 2] cycloaddition of arynes and sydnones, Fe-catalyzed N—N bond formation of 2-azidophenyl ketoximes, reaction of 2-chloromethylarylzinc reagents and aryldiazonium salts, one-pot condensation–Cadogan reductive cyclization from 2-nitrobenzaldehyde, Rh(III)-catalyzed C—H functionalization followed by cyclative capture, and Rh(III)-catalyzed [4 + 1] annulation of azoxy compounds with alkynes or diazo esters.[11] In 2011, Lee and co-workers developed a Cu(I)-catalyzed multicomponent approach to 2H-indazole derivatives from 2-bromobenzaldehyde.[12] More recently, Sharghi and Aberi used Cu₂O nanoparticles for indazole synthesis, albeit with limited substrate scope with no recyclability.[13] Most of the methods described above involve the consecutive formation of C—N and N—N bond for the synthesis of 2H-indazole derivatives, representing one of the most efficient and atom-economical synthetic strategy in modern organic synthesis and green chemistry. Nonetheless, most of these synthetic methodologies have drawbacks, such as the use of expensive Pd and Rh catalysts with ligands, longer reaction times, harsh reaction conditions, decomposition of substrates owing to overheating, and the problem of regioisomers, which is problematic for industrial use due to high cost and waste disposal. To overcome these drawbacks, and to extend them as green and environmentally friendly alternatives to the above-mentioned synthetic sequences, great progress has been made recently with new nanoparticle-based catalytic systems.

Recently, it was discovered that inorganic nanoparticles with high surface-to-volume ratio and exposed surface features provide excellent catalytic activity with high product selectivity.[14] Cu₂O nanocrystals of a variety of shapes have been widely pur-

[a] R. L. Panchangam, Prof. V. Manickam
Department of Biosciences, School of Bioscience and Technology, Vellore Institute of Technology, Vellore 632014 (India)
E-mail: venkatraman.m@vit.ac.in

[b] Prof. K. Chanda
Department of Chemistry, School of Advanced Sciences, Vellore Institute of Technology, Vellore 632014 (India)
E-mail: chandakaushik1@gmail.com

Supporting information and the ORCID identification number(s) for the author(s) of this article can be found under:
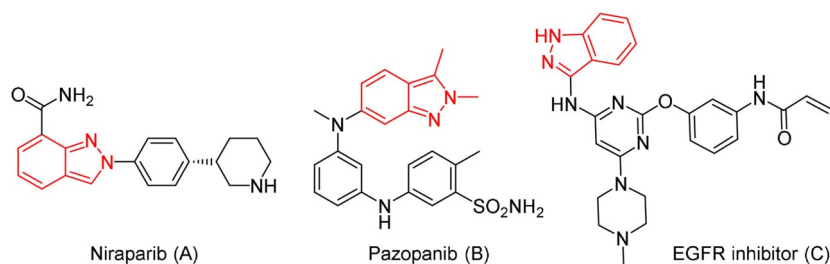https://doi.org/10.1002/cmdc.201800707.

Figure 1. Biologically active 2*H*-indazole-containing compounds.

sued for important organocatalytic, electrical conductivity, and photocatalytic properties.[15] According to the principles of green chemistry, the use of nanocatalysts attempts to decrease energy consumption and to optimize the use of the available resources, with the aim of it becoming a sustainable strategy for chemical transformations. In the form of nanoparticles, the exposed surface area of the active component of the catalyst is increased, depending on their shape, thereby dramatically increasing the contact between reactants and catalyst, which in turn mimics homogeneous catalysts by preserving the essential features of a heterogeneous catalyst. Recently, we demonstrated the effectiveness of Cu₂O rhombic dodecahedra nanocrystals for the one-pot regioselective synthesis of 1,4-disubstituted triazoles and 3,5-disubstituted isoxazoles in green media.[16] Furthermore, in 2014, for the first time we also performed 1,3-dipolar cycloaddition for the synthesis of 1,2,3-triazoles in water by the use of Au nanocrystals.[17]

Regarding the wide array of applications of 2*H*-indazole derivatives, as well as the catalytic importance of Cu₂O rhombic dodecahedra for synthetic manipulations, we envisioned that a C−N and N−N bond-forming reaction to give 2*H*-indazole derivatives should be readily feasible. In a continuation of our research to develop new synthetic methodologies for the construction of bioactive heterocycles,[18] herein, we report a novel Cu₂O rhombic dodecahedra-catalyzed synthesis of 2*H*-indazole derivatives under mild conditions. This reaction proceeds well under mild conditions and provides a good range of products in excellent yields with excellent regioselectivity. In addition, it avoids the requirement of high temperature, and the reaction tolerates both electron-donating and electron-withdrawing substituents, which make this protocol useful for the preparation of a series of 2*H*-indazole derivatives that can be further exploited for many applications. Furthermore, the synthesized compounds were evaluated for potential anticancer activity and by live cell imaging.

Results and Discussion

At the start of our study, Cu₂O rhombic dodecahedra were synthesized in aqueous solution by following our previously reported procedures.[16a] Exact amounts of a CuCl₂ solution as precursor, sodium dodecyl sulfate surfactant, NaOH solution, and hydroxylamine hydrochloride as a reducing agent were mixed at room temperature and left for 1 h to allow particle growth and to yield the rhombic dodecahedral Cu₂O particles. To evaluate the particle shape, scanning electron microscopy

(SEM) was performed on the synthesized Cu₂O rhombic dodecahedra, which, according to size distribution histograms, had an average particle size of approximately 340 nm (Figure 2). Both the crystal structure and composition of the obtained sample were analyzed by X-ray diffraction (XRD), which revealed an XRD pattern consistent with rhombic dodecahedra with exceptionally strong (110) and (220) peaks resulting from their {110} surface facets.
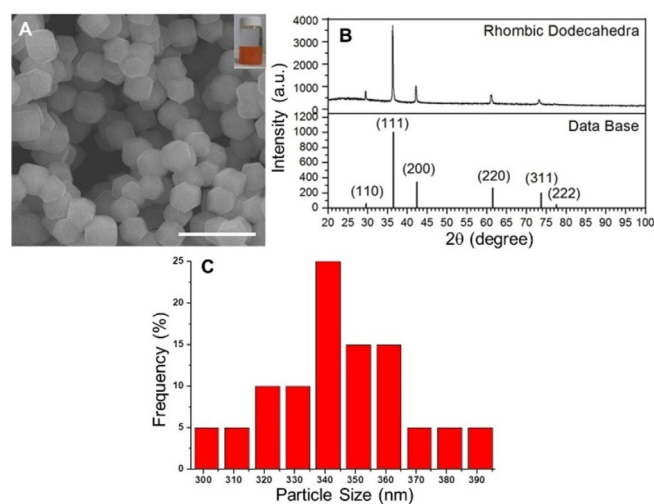

Figure 2. A) SEM images of synthesized rhombic dodecahedral Cu₂O nanocrystals. Scale bars: 1 μm. B) XRD patterns of the synthesized Cu₂O rhombic dodecahedra. A standard diffraction pattern of Cu₂O is also shown (JCPDS card no. 77–0199 for cuprite Cu₂O with a lattice constant a_o of 4.26 Å). Rhombic dodecahedra show enhanced (110) and (220) peaks as a result of their {110} faces. C) Size distribution histograms of Cu₂O rhombic dodecahedra with an average size of 340 ± 28 nm.

To establish the optimal reaction conditions, for our initial screening experiment, we chose the Cu₂O rhombic dodecahedra as a catalyst based on our earlier synthesis of 1,4-triazoles and isoxazoles.[16a, b] The catalytic activity of Cu₂O rhombic dodecahedra was examined in a model reaction between 2-bromobenzaldehyde (**1a**), NaN₃, and aniline (**2a**) in EtOH as solvent heated at reflux for 10 h (Table 1, entry 1). Disappointingly, only unreacted starting materials **1a** and **2a** were recovered from the reaction mixture. Unfortunately, the reaction did not afford any cyclized product using polar aprotic solvents such as CH₃CN or THF (Table 1, entries 2 and 3). Changing the solvent to DMF at 80 °C did not yield cyclized product **3a**

Table 1. Optimization of nanosized Cu₂O rhombic dodecahedra-catalyzed reaction of 2-bromobenzaldehyde (**1 a**), aniline (**2 a**), and NaN₃.[a]
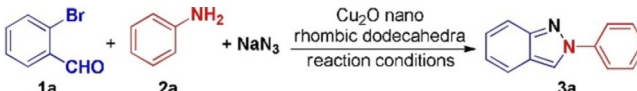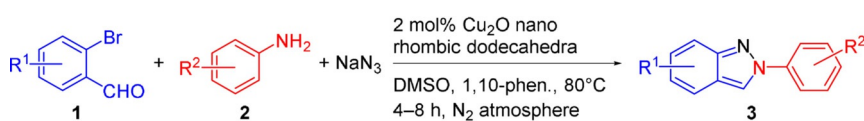

Entry	Ligand	Solvent	Temperature	Time	Yield[b]
1	–	EtOH	reflux	10 h	0%
2	–	CH₃CN	reflux	10 h	0%
3	–	THF	reflux	10 h	0%
4	–	DMF	80 °C	8 h	0%
5	1,10-Phen.	DMF	80 °C	8 h	0%
6	–	DMSO	80 °C	8 h	60%
7	1,10-Phen.	DMSO	80 °C	4 h	95%
8	1,10-Phen.[c]	DMSO	80 °C	4 h	95%

[a] Reaction was performed using **1 a** (1 mmol), **2 a** (1.2 mmol), NaN₃ (1.5 mmol). [b] Yields of isolated products. [c] Reaction was carried out using 5 mol% of Cuᴵ catalyst.

Table 2. Substrate scope of the reaction and physical properties of compounds **3**.[a]

Compd	R¹	R²	Yield[b]	HBD[c]	HBA[d]	clog P[e]	E-factor
3 a	H	Ph	95%	0	2	3.58	1.16
3 b	H	4-OCH₃C₆H₄	92%	0	3	3.75	1.13
3 c	4-F	Ph	84%	0	2	3.79	1.31
3 d	H	4-CH₃C₆H₄	93%	0	2	4.0	1.15
3 e	4-F	4-CH₃C₆H₄	86%	0	2	4.29	1.23
3 f	H	C₆H₅CH₂CH₂	88%	0	2	3.73	1.21
3 g	4-OCH₃	Ph	92%	0	3	3.70	1.07
3 h	4-CH₃	Ph	95%	0	2	4.07	1.08
3 i	4-OCH₃	C₆H₅CH₂CH₂	90%	0	3	3.86	1.03
3 j	4-OCH₃	4-CH₃C₆H₄	94%	0	3	3.70	0.99
3 k	4-OCH₃	4-OCH₃C₆H₄	94%	0	4	3.73	0.94
3 l	4-CH₃	4-CH₃C₆H₄	95%	0	2	4.57	1.03
3 m	4-CH₃	4-OCH₃C₆H₄	95%	0	3	4.25	0.98
3 n	H	4-CH(CH₃)₂C₆H₄	94%	0	2	5.0	1.15
3 o	H	3,4-(OCH₃)₂C₆H₃	93%	0	4	3.40	0.99
3 p	4-CH₃	4-CH(CH₃)₂C₆H₄	94%	0	2	5.5	0.85
3 q	4-CH₃	3,4-(OCH₃)₂C₆H₃	94%	0	4	3.90	0.93
3 r	4-OCH₃	3,4-(OCH₃)₂C₆H₃	90%	0	5	3.34	0.95
3 s	H	4-CF₃C₆H₄	78%	0	2	4.61	1.34

[a] Reaction conditions: 2-bromobenzaldehyde **1** (1 mmol), amine **2** (1.2 mmol), NaN₃ (1.5 mmol), catalyst (2 mol%), and 1,10-phenanthroline (2 mol%) were reacted in DMSO (4 mL) at 80 °C for 4–8 h. [b] Yields of isolated products. [c] Number of hydrogen bond donors. [d] Number of hydrogen bond acceptors. [e] clog P estimated using ChemBioOffice 2010.

(Table 1, entry 4). Adding the N-containing ligand 1,10-phenanthroline in DMF at 80 °C for 10 h did not yield any cyclized product (Table 1, entry 5). However, by changing the solvent system to DMSO at 80 °C, the reaction was completed in 8 h with a 60% yield (Table 1, entry 6). Surprisingly, to our delight, it was found that the desired product **3 a** was obtained in better yield if the reaction was performed in DMSO at 80 °C for only 4 h using 1,10-phenanthroline as ligand (95% yield, Table 1, entry 7). In an attempt to improve the yield of cyclized product **3 a**, increasing the catalyst loading to 5 mol% did not lead to any further improvements (Table 1, entry 8).

Finally, the optimized reaction conditions were found to be 2 mol% of nanosized Cu₂O rhombic dodecahedra (catalyst), DMSO (solvent), and 1,10-phenanthroline (ligand) at 80 °C for 4 h. With the optimized reaction conditions in hand, we next scrutinized the scope of the reaction using various aldehydes and amines. The use of various aromatic and aliphatic amines in the above reaction yielded a series of 2H-indazoles (Scheme 1 and Table 2). Interestingly, the reaction efficiency was unaffected by the substituent groups on either substituted 2-bromobenzaldehydes **1** or aromatic amines **2**. In the case of **2** having electron-neutral and electron-donating groups, such as aniline, p-toluidine, p-anisidine, and p-isopropylaniline, excellent yields were obtained. Aromatic amines with electron-withdrawing groups, such as 4-trifluoromethyl, gave poor yields. The low yield might be due to the difficulty in forming the imine intermediate in the reaction between aromatic aldehyde and aniline. Similarly, aliphatic amines or sterically hindered amines gave the corresponding 2H-indazole derivatives **3** in good yields. All these reactions were performed under a nitrogen atmosphere. The overall reaction time was typically 4–8 h.

After completion of the reaction, the corresponding 2H-indazole derivatives were obtained with excellent yields after a simple work-up involving filtration of the catalyst, removal, extraction, and solvent evaporation under reduced pressure. Finally, the crude products were purified by column chromatography and then spectroscopically characterized using analytical techniques. The results are summarized in Table 2. Recently, it has been realized that we need broad and global transformation strategies for sustainable chemistry, which can contribute to sustainable development through efficient, economical and ecofriendly chemical synthetic methods. In this context, Sheldon introduced the E-factor, or environmental impact factor, which is measured according to the waste produced in the process as opposed to the reaction.[19] Interestingly, our green synthetic reaction conditions for synthesizing many of the 2H-indazoles **3** have lower E-factors (Table 2), which is consistent with the principles of atom economy.
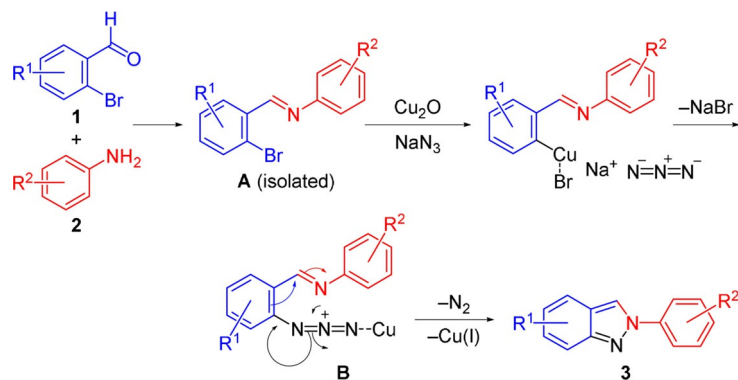
Furthermore, by using Lipinski's rule of five,[20] we calculated the physicochemical properties of the synthesized library to compute the oral bioavailability of the candidate drugs. These rules state that if the molecular weight is less than 500 Da, the clog P value, which addresses bioavailability and delivery issues, is not more than 5, there are not more than five hydrogen-bond donors, and the hydrogen-bond acceptors and ro-

Scheme 1. Synthesis of nano-Cu₂O rhombic dodecahedra-catalyzed disubstituted 2H-indazoles **3**.

tatable bonds are not more than 10 in number, then that potential molecule can have drug-like physical properties. However, one Lipinski violation is allowed for the design of a potential molecule. Fortunately, the predicted values of drug-like properties for these 2H-indazole derivatives are within the accepted limits of Lipinski's rule of five (Table 2).

The heterogeneous nature of the Cu_2O rhombic dodecahedra was confirmed by performing an additional experiment. The hot filtration experiment was carried out using Cu_2O rhombic dodecahedra as the catalyst.[21] In the control experiment, Cu_2O rhombic dodecahedra-catalyzed heterocyclization was carried out at 80 °C for 2 h followed by filtration at the reaction temperature. The supernatant solution was returned to the reaction vessel and the reaction was continued for another 2 h, which showed no catalytic activity. The filtered Cu_2O nanoparticles were re-dispersed in fresh DMSO solution containing fresh substrate and catalyzed the new reaction with almost the same activity (Figure S1 in the Supporting Information). The filtration study clearly rules out any possible contribution of homogeneous catalysis by leached Cu^I species in this cyclization reaction, so the observed catalytic activity is indeed due to heterogeneous catalysis.

A plausible mechanistic pathway for this heterocyclization reaction is outlined in Scheme 2. The first step of the reaction involves the formation of imine intermediate **A** from the reaction of 2-bromobenzaldehyde **1** and amine **2**, followed by the activation of Br by the Cu^I catalyst and azide ion to form the copper–azide complex **B**. The intermediate **B** then underwent electronic reorganization followed by the removal of molecule of N_2 and regeneration of the Cu^I catalyst to form the 2H-indazole derivative **3**. Furthermore, the Cu_2O rhombic dodecahedral nanocatalyst could be effectively recycled and reused in one further consecutive catalytic cycle with a product yield of 80%.

Because potent anticancer activity has been reported for other indazole derivatives,[22] we undertook a preliminary screening of all synthesized compounds **3a–s** for their cytotoxic activity against a panel of cancer cell lines, that consisted of human colon carcinoma (HCT116), human lung carcinoma (A549), and human breast carcinoma (MDA-MB-468), by using the 3-(4,5-dimethylthiazol-2-yl)-2,5-diphenyltetrazolium bro-

mide (MTT) assay. The results of this cytotoxicity assay, expressed as IC_{50} values, are summarized in Table 3. The commonly used wide-spectrum anticancer drug cisplatin was used as a positive control. The absorbance of the colored formazan

Table 3. Half-maximum inhibitory concentrations of synthesized 2H-indazole derivatives.

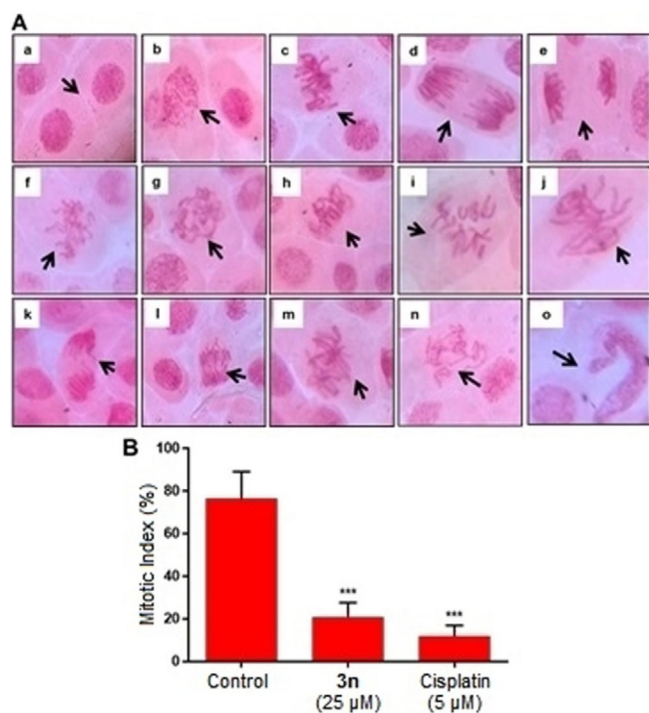| Compd	IC_{50} [μM][a]		
	A549[b]	MDA-MB-468[c]	HCT116[d]
3a	>100	97.7 ± 1.5	96.2 ± 1.5
3b	98.5 ± 3.0	>100	95.7 ± 2.3
3c	98.1 ± 3.0	49.4 ± 2.1	72.5 ± 1.3
3d	45.6 ± 2.0	32.5 ± 1.7	44.2 + 3.5
3e	94.3 ± 4.3	46.8 ± 3.2	98 ± 4.0
3f	>100	58.2 ± 2.5	73.1 ± 3.6
3g	>100	54.2 ± 3.0	98.3 ± 3.0
3h	>100	58.7 ± 1.9	80.7 ± 2.1
3i	37.2 ± 0.6	30.2 ± 3.1	50 ± 2.6
3j	>100	>100	75.8 ± 2.8
3k	50 ± 2.5	35.6 ± 0.8	67.1 ± 3.0
3l	>100	>100	>100
3m	50.6 ± 2.4	45.7 ± 1.2	48.6 ± 2.0
3n	37.1 ± 2.0	25.0 ± 2.5	26.1 ± 3.4
3o	40.4 ± 0.8	42.6 ± 1.8	50.2 ± 3.1
3p	29.0 ± 3.8	29.4 ± 1.2	40.5 ± 2.1
3q	57.2 ± 1.9	50.8 ± 2.1	67.9 ± 3.2
3r	35.9 ± 2.0	39.6 ± 0.8	37.6 ± 1.8
3s	>100	>100	>100

[a] IC_{50} values are averages ± SD of three individual experiments. [b] Lung cancer cells. [c] Breast cancer cells. [d] Colon cancer cells.

crystals formed after 48 h treatment of 2H-indazole compounds was measured at 570 nm. Among the 19 different 2H-indazole derivatives screened, isopropyl-substituted compound **3n** was found to have maximal cytotoxic effect in a concentration-dependent manner, and had IC_{50} values of 26.1, 37.1 and 25 μM in HCT116, A549 and MDA-MB-468 cell lines, respectively. We chose the effective IC_{50} concentration of 25 μM for further anticancer characterization studies with MDA-MB-468 cells.

It is well established that cancer is a disease caused by uncontrolled cell division whereby neoplastic cells undergo repeated mitosis. Mitosis is a stage of the cell cycle in which the cell genome is duplicated and followed by cytokinesis. Typically, classical anticancer drugs effectively kill all the fast-proliferating cells by mediating DNA damage that cannot be repaired. These chromosomal alterations can be readily evaluated in an anti-mitosis study using *Allium cepa* root tip cells.

We clearly confirmed the presence of chromosomal aberrations and other nuclear abnormalities in onion root tip cells treated with compound **3n** at 25 μM concentration; the results were similar to the cisplatin-treated positive controls (Figure 3 and Table 4). Relative to the negative control, compound **3n** (25 μM) gave a decrease in the mitotic index.
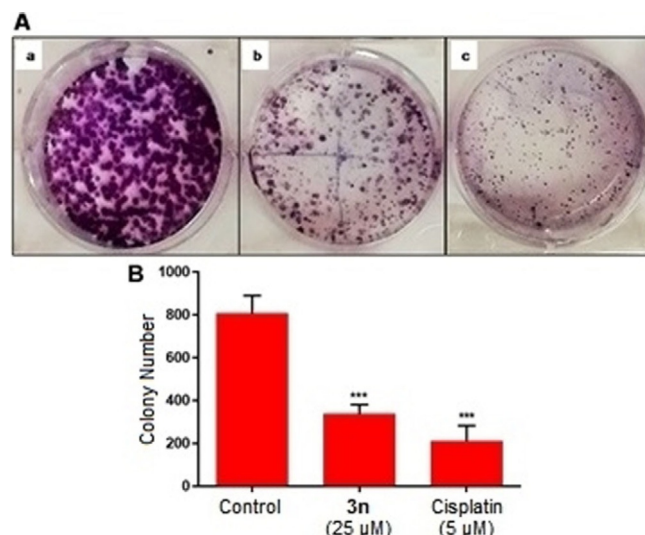
To confirm the effect of compound **3n** on the proliferation of MDA-MB-468 cells, a colony formation

Scheme 2. Possible mechanism for heterocyclization reaction to form 2H-indazole derivatives **3**.

Figure 3. Compound **3n** induces chromosomal aberrations in *Allium cepa* root tip cells. A) a–e: Untreated control cells showing normal mitotic phases—interphase (a), prophase (b), metaphase (c), anaphase (d), and telophase (e); f–o: cells showing aberrations upon treatment with **3n** (25 μм)—sticky prophase (f and g), h) spindle disturbance at metaphase (h), c-mitosis and fragmented chromosomes at metaphase (i), sticky metaphase (j), bridges at anaphase (k–n), and nuclear abnormalities (o). B) Histogram representing the percentage mitotic index versus drug concentration. Images are representative of three independent experiments and data are reported as the mean±SD; ***$P < 0.001$ versus control.


Figure 4. Effect of **3n** on the colony-formation ability of MDA-MB-468 cells in vitro. A) The results of colony formation: control (a), MDA-MB-468 cells treated with 25 μм **3n** (b), and cells treated with 5 μм cisplatin (c). Fewer colonies formed and those colonies were significantly smaller upon treatment with 25 μм **3n** relative to control. B) Histograms representing the number of colonies formed after 7 days of treatment. Images are representative of three independent experiments and data are reported as the mean±SD; ***$P < 0.05$ versus control.

assay was carried out. The extent of cancer cells to produce colonies if plated at low densities is related to their potential to proliferate, and the cytotoxic ability of a test compound correlates well with the inhibition of colony formation.[23] MDA-MB-468 cells treated with **3n** at a concentration of 25 μм showed a significant decrease in the number of colonies relative to untreated control cells (Figure 4A). The decrease in the colonies formed after treatment with **3n** was similar to that of the positive control cisplatin.

Apoptosis and necrosis are the principal modes of cell death, and of these, apoptosis is preferred in any cancer treatment. Apoptosis is a programmed cell death that efficiently removes dysfunctional cells; one hallmark property of cancer is the ability of cancer cells to evade apoptosis.[24] Using ethidium bromide (EtBr) and acridine orange (AO) double staining, we tested the ability of compound **3n** to induce apoptotic cell death in MDA-MB-468 cells. Using fluorescence microscopy, we showed the presence of cells bearing apoptotic nuclei after 24 h of treatment with compound **3n** at a concentration of 25 μм, which confirmed cell death by apoptosis. As shown in Figure 5a, the untreated control MDA-MB-468 cells appeared uniformly green in color, whereas at 24 h post-treatment with compound **3n** (25 μм), cells were both early apoptotic and late apoptotic (Figure 5b, EA and LA, respectively). Only late apoptotic cells were observed after treatment with cisplatin at a concentration of 5 μм (Figure 5c).

By this assay, it is evident that the compound **3n**, administered at a concentration of 25 μм, promoted apoptotic changes such as nuclear fragmentation in MDA-MB-468 cells, which can be equated with cisplatin-induced changes. Thus, these results suggest the efficacy of compound **3n** is similar to the commonly available anticancer drugs. This apoptosis-related cell death was further evaluated by analyzing the disruption of mitochondrial membrane potential and activation of caspases 3 and 7.

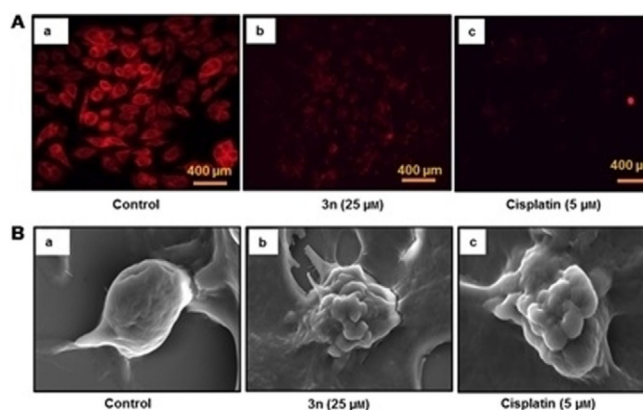| Table 4. Mitotic indices.								
Treatment	Total cells	Number of cells by mitotic phase				Total mitotic cells	Mitotic index [%]	No. aberrant mitotic cells	Aberrant mitotic cells [%]
		Prophase	Metaphase	Anaphase	Telophase				
Control	490	96	116	78	25	315	64.2857	0	0
25 μм	390	29	15	17	0	51	13.0769	51	100
Cisplatin	419	17	5	4	0	26	6.2052	26	100
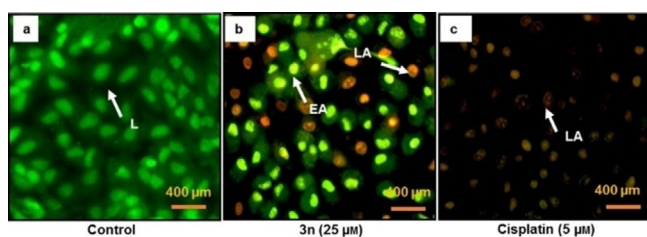
Figure 5. Compound **3n** induces cellular apoptosis in MDA-MB-468 cells. The MDA-MB-468 cells were stained with ethidium bromide and acridine orange: control live (L) cells (a), cells treated with 25 μM **3n**, including both early apoptotic (EA) and late apoptotic (LA) stages, and cells treated with 5 μM cisplatin showing late apoptotic cells (c). Images are representative of three independent experiments.

Figure 6. A) Effect of compound **3n** on mitochondrial membrane potential of MDA-MB-468 cells. Cells were stained with TMRE to assess mitochondrial membrane potential: control cells (a), cells treated with 25 μM **3n** (b), cells treated with 5 μM cisplatin (c). Images are representative of three independent experiments. B) The induction of apoptotic morphology of MDA-MB-468 cells by **3n** was evaluated by SEM analysis: control (a), cells treated with compound 25 μM **3n** (b), cells treated with 5 μM cisplatin (c). Images are representative of three independent experiments.
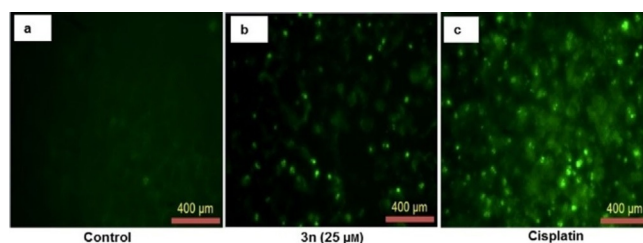
Mitochondrial outer membrane permeabilization and disruption of mitochondrial transmembrane potential are frequently used as markers of apoptosis. Intact and functional mitochondria are key indicators of cellular health, which can be assessed by monitoring the changes in mitochondrial membrane potential. During ATP synthesis by oxidative phosphorylation, positively charged protons are transferred across the inner membrane of mitochondria, resulting in a net negative mitochondrial membrane potential ($\Delta\Psi_m$). The membrane potential of healthy mitochondria is strictly maintained at -180 mV. Tetramethylrhodamine ethyl ester perchlorate (TMRE) is a positively charged fluorescent dye that readily diffuses specifically into mitochondrial membranes due to the negative charge generated by the mitochondrial membrane potential.[25] In this study, the treatment of MDA-MB-468 cells with 25 μM **3n** caused disruption in the mitochondrial membrane potential, and thus effectively decreased the fluorescence intensity relative to control cells having uniform bright fluorescence. A similar effect was observed in the cells treated with the positive control cisplatin at 5 μM (Figure 6 A).

During the execution phase of apoptosis, certain changes in cell morphology occur, which include cellular and nuclear contraction, and membrane blebbing.[26] The activation of caspase 3 is said to be the necessary driving event for membrane blebbing.[27]

Caspases are cysteine-aspartic proteases, which play important roles in apoptosis. During apoptosis, inactive initiator procaspases becomes rapidly cleaved and activated. Activated caspases in turn cleave a variety of downstream targets, such as effector caspases and nuclear, mitochondrial, and plasma membrane proteins, thus ultimately leading to programmed cell death.[28] In this study, to determine whether the cytotoxic effects of compound **3n** on MDA-MB-468 cells are caused by apoptosis, effector terminal caspase 3/7 activity was checked by using the CellEvent caspase 3/7 green detection reagent. This reagent contains a nucleic acid binding dye, which emits bright green fluorescence upon binding to DNA after the release of the inhibitory peptide DEVD. In apoptotic cells, the activated caspases 3 and 7 will cleave the DEVD peptide, allowing the free dye to bind to DNA and fluoresce. As shown in Figure 7, no bright green fluorescence was observed in the control cells, which indicated apoptosis had not occurred.


Figure 7. Effect of compound **3n** on activation of caspases 3 and 7 in MDA-MB-468 cells. Cells were stained with CellEvent Caspase 3/7 Green ReadyProbes Reagent (Invitrogen) to determine the activity of caspases 3 and 7: control cells (a), cells treated with 25 μM **3n** (b), cells treated with 5 μM cisplatin (c). Images are representative of three independent experiments.

However, the cells treated with compound **3n** at a concentration of 25 μM showed bright green fluorescence, indicating the activation of caspases 3 and 7 and apoptosis. Similar results were also observed in breast cancer cells (MDA-MB-468) treated with cisplatin at 5 μM.

It is well known that cellular migration and invasion play a crucial role in cancer metastasis. Pathogenesis and eventual cancer-related death are due to the spread of cancer cells from the primary site to other secondary sites during the advanced stages of malignancy. This metastatic process involves the migration and invasion of potent cancer cells into adjacent tissues and organs through blood and lymphatic vessels.

In this regard, to further ascertain the effect of compound **3n** on migration of MDA-MB-468 cells, we performed an in vitro wound-healing assay.[29] The wounds made were almost of same size for each experimental cell group at 0 h (Figure 8). The wound-healing assay demonstrated that 25 μM **3n** could markedly inhibit the migration and wound-closure capacity of MDA-MB-468 cells relative to those of control cells at 24 h. A similar effect was also observed for cells treated with the positive control cisplatin at 5 μM. The results of this assay illustrat-
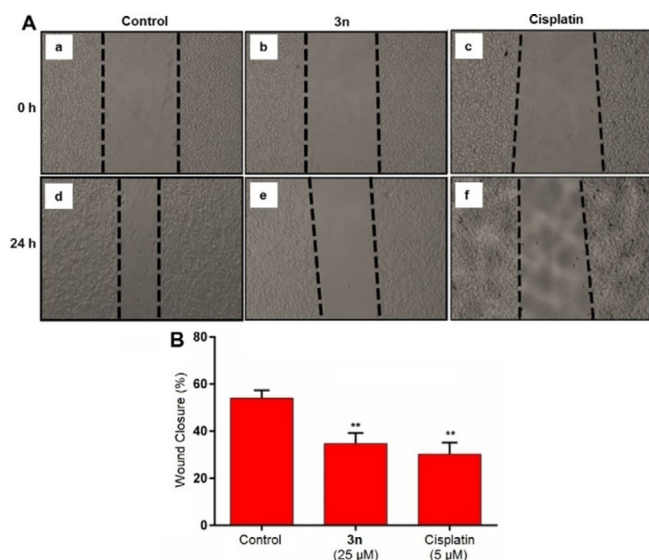
Figure 8. Compound **3n** inhibits the migration of MDA-MB-468 cells. A) Images showing **3n** inhibiting the migration of MDA-MB-468 cells. The black dotted lines indicate the wound borders. Images are representative of three independent experiments. B) Histograms representing the percentage wound closure at 24 h relative to the beginning of treatment (0 h). Data are the mean ± SD; **$P < 0.05$ versus control.

ed the possible inhibitory effect of the isopropyl-substituted 2*H*-indazole **3n** on cancer metastasis, which has to be evaluated further.

Overall, these results indicated the potential efficacy of isopropyl-substituted 2*H*-indazole compound **3n** as an anticancer treatment. MTT assays showed that **3n** inhibited the growth of A549, MDA-MB-468, and HCT116 cells in a time- and dose-dependent manner. The anti-proliferative effect of **3n** was further evidenced by the colony formation assay. Apoptosis induced by **3n** is mediated through the mitochondrial pathway as loss of mitochondrial membrane potential resulted from the activation of caspases 3 and 7. Compound **3n** also suppressed the migration and invasion of MDA-MB-468 cells. Resistance to cell death, unlimited replicative potential, clonal propagation, migration and tissue invasion are prominent features of cancer cells.[30] Malignant pathology is the result of these features, and therefore targeting these crucial processes provides a perfect strategy to control and destroy cancers. Our results indicate that a 2*H*-indazole derivative, **3n**, possessed significant anticancer activity and that further development of such compounds might be of interest to medicinal chemists.

Conclusions

We developed a Cu$_2$O rhombic dodecahedra-catalyzed heteroannulation strategy for clean synthesis of 2*H*-indazoles with excellent yields. The salient features of this strategy include milder reaction conditions, inexpensive reagents, high atom economy, and clean reaction profiles in a single synthetic operation. These synthesized compounds were evaluated for their in vitro anticancer activity. Biological activity data indicated that a compound with 4-isopropyl substituent on the 2*H*-inda-

zole moiety showed significant inhibitory activity on the growth of A549, MDA-MB-468, and HCT116 cancer cells in a time- and dose-dependent manner, which was evidenced further by induction of apoptosis, interruption of cancer cell colony formation, blocking of root-tip mitosis, and favored death through extensive chromosomal aberrations. Furthermore, the compound suppressed the in vitro migration and invasion potential of cancer cells. These results suggested that with the inherent cytotoxic activity, these heterocyclic molecules might serve as interesting lead compounds for the development of new anticancer agents. Further medicinal characterization and applications of the 2*H*-indazole derivatives are currently under investigation in our laboratory.

Experimental Section

Chemistry

Unless otherwise indicated all common reagents and solvents were used as obtained from commercial suppliers without further purification. ^{1}H NMR (300, 400, and 600 MHz) and ^{13}C NMR (75, 100, and 150 MHz) were recorded on Bruker DRX300 and Bruker DRX600 spectrometers. Chemical shifts are reported in ppm relative to the internal solvent peak. Coupling constants *J* are expressed in Hz. Multiplicities of peaks are given as: d (doublet), m (multiplet), s (singlet), and t (triplet). Mass spectra were recorded on a Perkin-nElmer Clarus 600 GC–MS spectrometer. High-resolution mass spectra were recorded in EI mode using a Jeol JMS-HX 110 mass spectrometer. IR spectra were recorded on a Bomem DA8 3FTS spectrometer. SEM images of samples were obtained using a Jeol JSM-700F electron microscope. Powder XRD patterns were recorded on a Shimadzu XRD-6000 diffractometer with CuKα radiation. TLC plates were Merck silica gel 60 F$_{254}$ on aluminum. Flash column chromatography was performed with silica gel (60–100 mesh).

General procedure for the synthesis of doubly substituted 2-aryl-2*H*-indazoles 3

In a round-bottomed flask under nitrogen atmosphere, a mixture of substituted 2-bromobenzaldehyde **1** (1.0 equiv), amine **2** (1.2 equiv) was added to DMSO (4 mL) followed by the addition of NaN$_3$ (1.5 equiv). The reaction mixture was stirred for 5 min at room temperature followed by the addition Cu$_2$O rhombic dodecahedra catalyst (2 mol%) and 1,10-phenanthroline (2 mol%) as a ligand. The reaction mixture was heated with stirring at 80 °C. The progress of the reaction was monitored by TLC. After completion, the reaction mixture was cooled to room temperature, filtered to remove the catalyst, and extracted with ethyl acetate (10 mL, twice). The combined organic layers were dried over anhydrous MgSO$_4$. The solvent was evaporated to obtain the crude compound, which was purified over a silica gel column (60–120 mesh) using 5–10% ethyl acetate in hexane as eluent to obtain the corresponding doubly substituted 2*H*-indazole **3** as the product.

2-Phenyl-2*H*-indazole (3a). Yield: 95%; white solid. ^{1}H NMR (400 MHz, CDCl$_3$): δ = 8.29 (s, 1H), 7.80 (d, *J* = 8.6 Hz, 2H), 7.71 (d, *J* = 8.8 Hz, 1H), 7.60 (d, *J* = 8.6 Hz, 1H), 7.42 (t, *J* = 7.6 Hz, 2H), 7.29 (t, *J* = 7.1 Hz, 1H), 7.23 (t, *J* = 7.5 Hz, 1H) 7.02 ppm (t, *J* = 7.16 Hz, 1H); ^{13}C NMR (100 MHz, CDCl$_3$): δ = 149.8, 140.5, 129.6, 128.1, 127.9, 126.8, 122.8, 122.4, 121.0, 120.4, 117.6 ppm; MS (GC–MS): *m/*

z: 194 [M]$^+$; HRMS (EI): m/z: calcd for C$_{13}$H$_{10}$N$_2$: 194.0844 [M]$^+$; found: 194.0846.

2-(4-Methoxyphenyl)-2H-indazole (3b). Yield: 92%; white solid. ^{1}H NMR (300 MHz, CDCl$_3$): δ = 8.33 (d, J = 1.0 Hz, 1H), 7.84–7.79 (m, 3H), 7.71 (dd, J = 8.4, 1.0 Hz, 1H), 7.37–7.34 (m, 1H), 7.15–7.10 (m, 1H), 7.04 (dd, J = 6.9, 2.0 Hz, 2H), 3.86 ppm (s, 3H); ^{13}C NMR (75 MHz, CDCl$_3$): δ = 159.7, 149.8, 134.5, 126.9, 122.9, 122.8, 122.6, 120.8, 120.7, 118.1, 115.0, 56.0 ppm; MS (GC–MS): m/z: 224 [M]$^+$; HRMS (EI): m/z: calcd for C$_{14}$H$_{12}$N$_2$O: 224.0950 [M]$^+$; found: 224.0951.

6-Fluoro-2-phenyl-2H-indazole (3c). Yield: 84%; pale brown solid. ^{1}H NMR (400 MHz, CDCl$_3$): δ = 8.41 (s, 1H), 7.86 (d, J = 7.6 Hz, 2H), 7.69 (dd, J = 8.8, 5.2 Hz, 1H), 7.53 (t, J = 7.6 Hz, 2H), 7.43–7.35 (m, 2H), 6.93 (dt, J = 9.0, 0.8 Hz, 1H), 3.86 ppm (s, 3H); ^{13}C NMR (100 MHz, CDCl$_3$): δ = 162.2 (d, J$_{CF}$ = 242 Hz, 1C), 149.5, 140.3, 129.6, 128.0, 122.3, 122.1. 120.8, 120.4, 114.5 (d, J$_{CF}$ = 29 Hz, 1C), 101.1 ppm (d, J$_{CF}$ = 23.7 Hz, 1C); MS (GC–MS): m/z: 212 [M]$^+$; HRMS (EI): m/z: calcd for C$_{13}$H$_9$FN$_2$: 212.0750 [M]$^+$; found: 212.0748.

2-(p-Tolyl)-2H-indazole (3d). Yield: 93%; white solid. ^{1}H NMR (400 MHz, CDCl$_3$): δ = 8.36 (s, 1H), 7.78 (t, J = 8.6 Hz, 2H), 7.70 (d, J = 8.5 Hz, 1H), 7.33 (t, J = 8.4 Hz, 3H), 7.11 (t, J = 8.0 Hz, 1H), 2.42 ppm (s, 3H); ^{13}C NMR (100 MHz, CDCl$_3$): δ = 149.6, 138.3, 137.9, 130.0, 126.6, 122.3, 120.9, 120.8, 120.4, 120.3, 117.8, 21.1 ppm; MS (GC–MS): m/z: 208 [M]$^+$; HRMS (EI): m/z: calcd for C$_{14}$H$_{12}$N$_2$: 208.1000 [M]$^+$; found: 208.0996.

6-Fluoro-2-(p-tolyl)-2H-indazole (3e). Yield: 86%; pale brown solid. ^{1}H NMR (400 MHz, CDCl$_3$): δ = 8.34 (d, J = 0.9 Hz, 1H), 7.72 (dd, J = 6.6, 2.0 Hz, 2H), 7.65 (d, J = 0.6 Hz, 1H), 7.30–7.23 (m, 2H), 6.90 (d, J = 2.0 Hz, 1H), 2.41 ppm (s, 3H); ^{13}C NMR (100 MHz, CDCl$_3$): δ = 162.8 (d, J$_{CF}$ = 243 Hz, 1C), 149.6, 138.1, 129.9 (t, J$_{CF}$ = 31.3 Hz, 1C), 122.2 (d, J$_{CF}$ = 31.3 Hz, 1C), 120.7, 114.2 9 (t, J$_{CF}$ = 28.5 Hz, 1C), 101.1 (d, J$_{CF}$ = 23.76 Hz, 1C), 21.0 ppm; MS (GC–MS): m/z: 226 [M]$^+$; HRMS (EI): m/z: calcd for C$_{14}$H$_{11}$FN$_2$: 226.0906 [M]$^+$; found: 226.0903.

2-Phenethyl-2H-indazole (3f). Yield: 88%; pale white solid. ^{1}H NMR (400 MHz, CDCl$_3$): δ = 7.75 (dd, J = 8.6, 1.2 Hz, 1H), 7.69 (s, 1H), 7.59 (dd, J = 8.6, 1.0 Hz, 2H), 7.32–7.24 (m, 4H), 7.10–7.05 (m, 3H), 4.42 (t, J = 7.6 Hz, 2H), 3.32 ppm (t, J = 7.6 Hz, 2H); ^{13}C NMR (100 MHz, CDCl$_3$): δ = 148.9, 137.7, 128.6, 128.5, 126.7, 125.8, 127.9, 121.5, 120.0, 117.3, 55.1, 37.0 ppm; MS (GC–MS): m/z: 222 [M]$^+$; HRMS (EI): m/z: calcd for C$_{15}$H$_{14}$N$_2$: 222.1157 [M]$^+$; found: 222.1160.

6-Methoxy-2-phenyl-2H-indazole (3g). Yield: 92%; white solid. ^{1}H NMR (600 MHz, CDCl$_3$): δ = 8.24 (s, 1H), 7.84 (dd, J = 7.6, 1.0 Hz, 2H) 7.65 (dd, J = 8.4, 1.0 Hz, 1H) 7.48 (dd, J = 7.4, 1.0 Hz, 1H), 7.36–7.34 (m, 1H), 7.01 (dd, J = 9.0, 2.1 Hz, 1H), 6.87 (d, J = 2.1 Hz, 1H), 3.83 ppm (s, 3H); ^{13}C NMR (150 MHz, CDCl$_3$): δ = 155.5, 146.7, 140.6, 129.5, 127.5, 122.8, 122.0, 120.6, 119.3, 119.2, 96.3, 55.3 ppm; MS (GC–MS): m/z: 224 [M]$^+$; HRMS (EI): m/z: calcd for C$_{14}$H$_{12}$N$_2$O: 224.0950 [M]$^+$; found: 224.0947.

6-Methyl-2-phenyl-2H-indazole (3h). Yield: 95%; white solid. ^{1}H NMR (600 MHz, CDCl$_3$): δ = 8.31 (d, J = 8.8 Hz, 1H), 7.87 (t, J = 1.0 Hz, 1H), 7.85 (dd, J = 1.2, 0.8 Hz, 1H), 7.57 (d, J = 8.6 Hz, 1H), 7.51–7.48 (m, 3H), 7.36 (t, J = 7.3 Hz, 1H), 6.93 (dd, J = 8.6, 1.2 Hz, 1H), 2.45 ppm (s, 3H); ^{13}C NMR (150 MHz, CDCl$_3$): δ = 150.4, 140.6, 1368, 129.5, 127.6, 125.5, 121.2, 120.8, 120.2, 119.9, 116.2, 22.3 ppm; MS (GC–MS): m/z: 208 [M]$^+$; HRMS (EI): m/z: calcd for C$_{14}$H$_{12}$N$_2$: 208.1000 [M]$^+$; found: 208.1002.

6-Methoxy-2-phenethyl-2H-indazole (3i). Yield: 90%; off white solid. ^{1}H NMR (600 MHz, CDCl$_3$): δ = 7.60 (d, J = 9.0 Hz, 1H), 7.55 (s, 1H), 7.26–7.24 (m, 2H), 7.21 (d, J = 7.3 Hz, 1H) 7.08 (dd, J = 8.3, 1.5 Hz, 2H), 6.97 (dd, J = 9.0, 2.4 Hz, 1H), 6.80 (d, J = 2.4 Hz, 1H), 4.55 (t, J = 7.4 Hz, 2H), 3.79 (s, 3H), 3.27 ppm (t, J = 7.4 Hz, 2H); ^{13}C NMR (150 MHz, CDCl$_3$): δ = 154.9, 145.7, 137.9, 128.7, 128.6, 126.7, 122.04, 121.4, 120.5, 118.7, 96.6, 55.3, 54.9, 37.1 ppm; MS (GC–MS): m/z: 252 [M]$^+$; HRMS (EI): m/z: calcd for C$_{16}$H$_{16}$N$_2$O: 252.1263 [M]$^+$; found: 252.1269.

6-Methoxy-2-(p-tolyl)-2H-indazole (3j). Yield: 94%; pale white solid. ^{1}H NMR (600 MHz, CDCl$_3$): δ = 8.17 (s, 1H), 7.70 (d, J = 8.3 Hz, 2H), 7.66 (dd, J = 9.0, 0.7 Hz, 1H), 7.25 (dd, J = 8.3, 0.7 Hz, 2H), 7.01 (dt, J = 7.3, 2.3 Hz, 1H), 6.84 (d, J = 2.3 Hz, 1H), 3.81 (s, 3H), 2.38 ppm (s, 3H); ^{13}C NMR (150 MHz, CDCl$_3$): δ = 155.4, 146.5, 138.3, 137.4, 129.9, 122.6, 121.7, 128.4, 119.2, 119.1, 96.3, 55.3, 20.9 ppm; MS (GC–MS): m/z: 252 [M]$^+$; HRMS (EI): m/z: calcd for C$_{15}$H$_{14}$N$_2$O: 238.1106 [M]$^+$; found: 238.1115.

6-Methoxy-2-(4-methoxyphenyl)-2H-indazole (3k). Yield: 94%; pale white solid. ^{1}H NMR (600 MHz, CDCl$_3$): δ = 8.12 (s, 1H), 7.72 (dd, J = 6.9, 2.2 Hz, 2H), 7.65 (d, J = 9.2 Hz, 1H), 6.99 (dd, J = 9.2, 2.2 Hz, 1H), 6.85 (d, J = 2.2 Hz, 1H), 6.97 (dd, J = 6.9, 2.2 Hz, 2H), 3.82 (s, 3H), 3.81 ppm (s, 3H); ^{13}C NMR (150 MHz, CDCl$_3$): δ = 158.9, 155.4, 146.4, 134.2, 122.6, 121.9, 121.5, 119.2, 119.1, 114.5, 96.3, 55.5, 55.3 ppm; MS (GC–MS): m/z: 254 [M]$^+$; HRMS (EI): m/z: calcd for C$_{15}$H$_{14}$N$_2$O$_2$: 254.1054 [M]$^+$; found: 254.1057.

6-Methyl-2-(p-tolyl)-2H-indazole (3l). Yield: 95%; pale yellow solid. ^{1}H NMR (600 MHz, CDCl$_3$): δ = 8.26 (s, 1H), 7.72 (d, J = 8.0 Hz, 2H), 7.55 (d, J = 8.3 Hz, 2H), 7.52 (s, 1H), 7.26 (dd, J = 8.0, 0.7 Hz, 2H), 6.93 (d, J = 8.3 Hz, 1H), 2.45 (s, 3H), 2.39 ppm (s, 3H); ^{13}C NMR (150 MHz, CDCl$_3$): δ = 150.2, 138.3, 137.5, 136.5, 129.9, 125.2, 121.0, 120.6, 120.0, 119.8, 116.1, 22.2, 20.9 ppm; MS (GC–MS): m/z: 222 [M]$^+$; HRMS (EI): m/z: calcd for C$_{15}$H$_{14}$N$_2$: 222.1157 [M]$^+$; found: 222.1154.

2-(4-Methoxyphenyl)-6-methyl-2H-indazole (3m). Yield: 95%; off-white solid. ^{1}H NMR (600 MHz, CDCl$_3$): δ = 8.19 (d, J = 1.0 Hz, 1H), 7.74 (dd, J = 6.9, 2.2 Hz, 2H), 7.54 (d, J = 8.6 Hz, 1H), 7.51 (dd, J = 2.2, 0.9 Hz, 1H) 6.97 (dd, J = 6.9, 2.2 Hz, 2H), 6.92 (dd, J = 8.6, 1.0 Hz, 1H), 3.82 (s, 3H), 2.45 ppm (s, 3H); ^{13}C NMR (150 MHz, CDCl$_3$): δ = 159.1, 150.2, 136.4, 134.1, 125.1, 122.2, 121.0, 120.0, 119.7, 116.0, 114.5, 55.5, 22.2 ppm; MS (GC–MS): m/z: 238 [M]$^+$; HRMS (EI): m/z: calcd for C$_{15}$H$_{14}$N$_2$O: 238.1106 [M]$^+$; found: 238.1105.

2-(4-Isopropylphenyl)-2H-indazole (3n). Yield: 94%; off-white solid. ^{1}H NMR (600 MHz, CDCl$_3$): δ = 8.34 (d, J = 1.0 Hz, 1H), 7.80–7.77 (m, 3H), 7.68 (dd, J = 8.5, 0.9 Hz, 1H), 7.35 (dd, J = 1.7, 2.0 Hz, 2H), 7.31–7.29 (m, 2H), 7.10–7.08 (m, 1H), 2.97 (q, J = 7.8 Hz, 1H), 1.29 (s, 3H), 1.27 ppm (s, 3H); ^{13}C NMR (150 MHz, CDCl$_3$): δ = 149.6,148.8, 138.5, 127.5, 126.6, 122.7, 122.3, 120.9, 120.3, 120.3, 117.9, 33.7, 23.9 ppm; MS (GC–MS): m/z: 236 [M]$^+$; HRMS (EI): m/z: calcd for C$_{16}$H$_{16}$N$_2$: 236.1313 [M]$^+$; found: 236.1312.

2-(3,4-Dimethoxyphenyl)-2H-indazole (3o). Yield: 93%; white solid. ^{1}H NMR (600 MHz, CDCl$_3$): δ = 8.22 (s, 1H), 7.74 (d, J = 8.8, Hz, 1H), 7.60 (d, J = 8.5 Hz, 1H), 7.47 (d, J = 2.3 Hz, 1H), 7.27–7.24 (m, 1H), 7.21 (dt, J = 8.5, 0.7 Hz, 1H), 7.04 (dd, J = 7.5, 0.8 Hz, 1H), 6.82 ppm (d, J = 8.8 Hz, 1H); ^{13}C NMR (150 MHz, CDCl$_3$): δ = 149.5, 149.3, 148.7, 134.1, 126.4, 122.5, 122.1, 120.3, 120.1, 117.5, 112.4, 111.1, 105.3, 56.0, 55.9 ppm; MS (GC–MS): m/z: 254 [M]$^+$; HRMS (EI): m/z: calcd for C$_{15}$H$_{14}$N$_2$O$_2$: 254.1055 [M]$^+$; found: 254.1060.

2-(4-Isopropylphenyl)-6-methoxy-2H-indazole (3p). Yield: 94%; white solid. ^{1}H NMR (600 MHz, CDCl$_3$): δ = 8.20 (d, J = 0.7 Hz, 1H), 7.76 (d, J = 8.5 Hz, 2H), 7.69 (d, J = 9.0 Hz, 1H), 7.34 (d, J = 8.5 Hz, 2H), 7.04 (td, J = 9.0, 1.5 Hz, 1H), 6.87 (d, J = 2.0 Hz, 1H), 3.83 (s,

3 H), 2.97 (m, 1 H), 1.30 (d, $J=1.8$ Hz, 3 H), 1.29 ppm (d, $J=1.8$ Hz, 3 H); ^{13}C NMR (150 MHz, CDCl$_3$): $\delta=155.4$, 148.4, 146.5, 138.5, 127.4, 122.6, 121.7, 120.5, 119.3, 119.1, 96.3, 55.2, 33.7, 23.8 ppm; MS (GC–MS): m/z: 266 [M]$^+$; HRMS (EI): m/z: calcd for C$_{17}$H$_{18}$N$_2$O: 266.1419 [M]$^+$; found: 266.1418.

2-(3,4-Dimethoxyphenyl)-6-methyl-2H-indazole (3 q). Yield: 94%; white solid. ^{1}H NMR (600 MHz, CDCl$_3$): $\delta=8.22$ (s, 1 H), 7.54 (d, $J=$ 8.5 Hz, 2 H), 7.49 (dd, $J=9.0$, 1.0 Hz, 1 H), 7.26–7.24 (m, 1 H), 6.92 (d, $J=8.5$ Hz, 1 H), 6.90 (d, $J=8.5$ Hz, 1 H), 3.96 (s, 3 H), 3.90 (s, 3 H), 2.44 ppm (s, 3 H); ^{13}C NMR (150 MHz, CDCl$_3$): $\delta=150.1$. 149.5, 148.6, 136.5, 134.3, 125.2, 120.9, 120.2, 119.7, 115.9, 112.4, 111.1, 105.3, 56.1, 56.0, 22.2 ppm; MS (GC–MS): m/z: 268 [M]$^+$; HRMS (EI): m/z: calcd for C$_{16}$H$_{16}$N$_2$O$_2$: 268.1212 [M]$^+$; found: 268.1209.

2-(3,4-Dimethoxyphenyl)-6-methoxy-2H-indazole (3 r). Yield: 90%; white solid. ^{1}H NMR (600 MHz, CDCl$_3$): $\delta=8.17$ (d, $J=0.9$ Hz, 1 H), 7.65 (d, $J=9.2$ Hz, 1 H), 7.48 (d, $J=2.5$ Hz, 1 H), 7.25 (dd, $J=$ 8.5, 2.5 Hz, 1 H), 7.00 (dd, $J=9.2$, 2.2 Hz, 1 H), 6.92 (d, $J=8.5$ Hz, 1 H), 6.87 (d, $J=2.2$ Hz, 1 H), 3.97 (s, 3 H), 3.91 (s, 3 H), 3.83 ppm (s, 3 H); ^{13}C NMR (150 MHz, CDCl$_3$): $\delta=155.4$, 149.7, 148.6, 146.5, 134.5, 122.7, 121.7. 119.4, 119.1, 112.3, 111.2, 105.3, 96.3, 56.2, 55.3 ppm; MS (GC–MS): m/z: 284 [M]$^+$; HRMS (EI): m/z: calcd for C$_{16}$H$_{16}$N$_2$O$_3$: 284.1161 [M]$^+$; found: 284.1162.

2-[4-(Trifluoromethyl)phenyl]-2H-indazole (3 s). Yield: 83%; yellow solid. ^{1}H NMR (400 MHz, CDCl$_3$): $\delta=8.47$ (s, 1 H), 8.06 (d, $J=$ 8.4 Hz, 2 H), 7.78 (t, $J=8.4$ Hz, 3 H), 7.71 (d, $J=8.5$ Hz, 1 H), 7.34 (t, $J=7.0$ Hz, 1 H), 7.13 ppm (t, $J=8.1$ Hz, 1 H); ^{13}C NMR (100 MHz, CDCl$_3$): $\delta=150.2$, 127.5, 126.9, 126.9, 126.8, 126.8, 123.0, 123.0, 120.7, 120.4, 118.0 ppm; MS (GC–MS): m/z: 262 [M]$^+$.

Biology

Chemicals and reagents

3-(4,5-Dimethylthiazol-2-yl)-2,5-diphenyltetrazolium bromide (MTT), ethidium bromide, acridine orange, acetocarmine, crystal violet, glacial acetic acid, and methanol were purchased from Himedia (Mumbai, India). TMRE and cisplatin were purchased from Sigma–Aldrich. CellEvent Caspase-3/7 Green ReadyProbes Reagent was purchased from Invitrogen.

Cell lines and cell culture conditions

Human colon cancer cells (HCT116), human lung cancer cells (A549), and human breast cancer cells (MDA-MB-468) were obtained from National Centre for Cell Sciences (NCCS), Pune, India. The cells were maintained in Dulbecco's modified Eagle's medium (Himedia) supplemented with 10% fetal bovine serum (Himedia), 100 µg mL^{-1} streptomycin, and 100 U mL^{-1} penicillin (Himedia) in a humidified incubator at 5% CO$_2$ and 20% O$_2$ at 37 °C.

Cell viability assay

The effect of novel 2H-indazoles on the viability of A549, HCT116, and MDA-MB-468 cells was analyzed by MTT assay with slight modifications from a reported procedure.[31] In brief, 1×10^4 cells were seeded in 96-well plates and after the cells reached about 70–80% confluency, the cells were treated with different concentrations of 2H-indazoles for 24 h. Cisplatin served as a positive control and DMSO was the untreated vehicle control. In all the treatments, final concentration of DMSO did not exceed more than 0.25% in the medium. After treatment, MTT (5 mg mL^{-1} in $1\times$ phosphate-buffered saline (PBS)) was added into each well and the cells were incubated for 4 h. Then, DMSO was added and the intensity of the purple color that formed was analyzed at 570 nm by using an ELISA plate reader (BioTek-ELx800). The IC$_{50}$ values were calculated by plotting percentage cell viability against drug concentration. All the experiments were performed in triplicate.

Allium cepa root tip assay

The antimitotic activity of compound 3 n was evaluated by using Allium cepa root tip cells in a slightly modified reported protocol.[32] The skins of onion bulbs were peeled, then the bulbs were placed on top of distilled water and roots were allowed to develop. After roots were formed, the bulbs were transferred to tubes containing compound 3 n and incubated for 24 h. Simultaneously, control bulbs were similarly maintained in distilled water without treatment with the drug. Cisplatin (5 µm) was used as a positive control. Root tips of around 2–3 mm were cut and fixed with Carnoy's fixative and hydrolyzed in HCl (1 N) for 15 min. The root tips were stained with acetocarmine solution and a squash was prepared. The images were acquired using an Olympus CKX41SF microscope. The mitotic index was calculated using Equation (1):

$$\text{Mitotic index} = \frac{\text{number of dividing cells}}{\text{total number of cells}} \times 100 \qquad (1)$$

Colony formation assay

To assess the effect of compound 3 n on the survival and proliferation of MDA-MB-468 cells, a colony formation assay was performed.[33] In brief, 1×10^3 cells per well were seeded in six-well plates and, after reaching 70%-80% confluency, the cells were treated with compound 3 n (25 µm) for 24 h; cisplatin (5 µm) was used as positive control. The untreated cells served as a control. Then, the cells were incubated for a further 14–20 days to allow the formation of colonies. Formed colonies were fixed with 4% paraformaldehyde and then stained with 0.5% crystal violet for 15 min. The number of colonies produced was counted manually.

Ethidium bromide and acridine orange double staining assay

To analyze the effect of 3 n on inducing apoptotic changes in MDA-MB-468 cells, an EtBr and AO double staining assay was performed with slight modifications to the reported procedure.[34] The MDA-MB-468 cells were grown on coverslips and then treated with compound 3 n (25 µm) for 24 h. Control cells were maintained untreated, and cisplatin (5 µm) was used as positive control. After incubation, a staining solution containing AO (100 µg mL^{-1}) and EtBr (100 µg mL^{-1}) was added to the cells, which were incubated for 5 min in darkness. Then, the cells were examined for their staining pattern under a fluorescence microscope (Weswox Optik-FM 3000).

Mitochondrial transmembrane potential ($\Delta \Psi_m$) analysis

To analyze the mitochondrial inner membrane depolarization caused by compound 3 n, a fluorescent dye staining was performed with slight modifications of the previously reported protocol.[35] MDA-MB-468 cells were grown on coverslips and incubated until they reached confluency. Then, the cells were treated with 3 n (25 µm) for 24 h. Control cells were maintained untreated, and cisplatin (5 µm) was used as positive control. A staining solution containing TMRE (150 nm) was applied to the coverslips and they were incubated for 20 min in darkness. Then, the coverslips were carefully placed on to a clean microscope slide and cells were examined

for their mitochondrial membrane depolarization under a fluorescence microscope (Weswox Optik-FM 3000).

Apoptotic morphological analysis by scanning electron microscopy

To evaluate the effect of compound **3n** on induction of apoptosis, a morphology analysis was performed by SEM. In brief, MDA-MB-468 cells were seeded at a minimal density on coverslips in multiwell culture plates and allowed to reach 70–80% confluency before treatment with **3n** (25 μм) or cisplatin (5 μм) for 24 h. The control cells were left untreated. After incubation, cells were washed three times with 1× PBS, and fixed for 2 h with 2.5% glutaraldehyde at 4 °C. Dehydration was performed with gradients of 30, 50, 70, 80, 90, 96, and 100% ethanol at 15 min intervals, and samples were left to dry for 48 h. The surfaces of the MDA-MB-468 cells were spray-coated with gold and examined by SEM (Zeiss Evo 18 microscope).

Detection of caspase 3/7 activity

Activation of caspases 3 and 7 was analyzed using CellEvent Caspase 3/7 Green ReadyProbes Reagent (Invitrogen). According to the manufacturer's protocol, 1×10^5 MDA-MB-468 cells were seeded on glass coverslips, placed in a six-well plate and treated with compound of **3n** (25 μм). The control cells were maintained without addition of compound **3n** and incubated for 24 h. After treatment, each well was loaded with two drops of CellEvent Caspase 3/7 Green ReadyProbes Reagent and incubated for 30 min at 37 °C. Then, the coverslips were removed from the wells and caspase-3/7-positive cells were analyzed using a fluorescence microscope (Weswox Optik-FM 3000).

In vitro wound healing migration assay

Analysis of the effect of compound **3n** on migration of MDA-MB-468, was performed by using a wound healing assay.[36] Cells were seeded at a density of 3×10^5 cells per well in a six-well plate and incubated for 24 h. A single wound was made on the plates by using a 200 μL sterile pipette tip. The plates were washed with sterile 1× PBS to remove cell debris and then treated with compound **3n** (25 μм) for 24 h. Control cells were maintained untreated, and cisplatin (5 μм) was used as positive control. Images were acquired at 0 and 24 h after the drug additions using an inverted microscope (MAGNUS 10J617). The area of the wound was measured by using ImageJ software. The migration of the cells into the wound area is represented as the percentage of wound closure relative to the size at 0 h. The percentage wound closure was calculated by using Equation (2):

$$\% \text{ Wound closure} = \frac{(\text{original scratch width}) - (\text{new scratch width})}{\text{original scratch width}} \times 100 \quad (2)$$

Statistical analysis

The values obtained in the experiments are expressed as the mean ± standard deviation (SD) and were analyzed by one-way analysis of variance (ANOVA) if appropriate, with a post-Dunnett's multiple comparisons test. A P value of <0.05 was considered statistically significant.

[1] a) D. M. D'Souza, T. J. J. Müller, *Chem. Soc. Rev.* **2007**, *36*, 1095–1108; b) F. Hu, M. Szostak, *Adv. Synth. Catal.* **2015**, *357*, 2583–2614.
[2] L. A. Clutterbuck, C. G. Posada, C. Visintin, D. R. Riddal, B. Lancaster, P. J. Gane, J. Garthwaite, D. L. Selwood, *J. Med. Chem.* **2009**, *52*, 2694–2707.
[3] S. Qian, J. Cao, Y. Yan, M. Sun, H. Zhu, Y. Hu, Q. He, B. Yang, *Mol. Cell. Biochem.* **2010**, *345*, 13–21.
[4] W. Han, J. C. Pelletier, C. N. Hodge, *Bioorg. Med. Chem. Lett.* **1998**, *8*, 3615–3620.
[5] X. Li, S. Chu, V. A. Feher, M. Khalili, Z. Nie, S. Margosiak, V. Nikulin, J. Levin, K. G. Sparankle, M. E. Fedder, R. Almassy, K. Appelt, K. M. Yager, *J. Med. Chem.* **2003**, *46*, 5663–5673.
[6] M. De Angelis, F. Stossi, K. A. Carlson, B. S. Katzenellenbogen, J. A. Katzenellenbogen, *J. Med. Chem.* **2005**, *48*, 1132–1144.
[7] J. Catalán, J. C. del Valle, R. M. Claramunt, G. Boyer, J. Laynez, J. Gómez, P. Jiménez, F. Tomás, J. Elguero, *J. Phys. Chem.* **1994**, *98*, 10606–10610.
[8] a) C. K. Chung, P. G. Bulger, B. Kosjek, K. M. Belyk, N. Rivera, M. E. Scott, G. R. Hunphery, J. Limanto, D. C. Bachert, K. M. Emerson, *Org. Process Res. Dev.* **2014**, *18*, 215–227; b) Y. Jia, J. Zhang, J. Feng, F. Xu, H. Pan, W. Xu, *Chem. Biol. Drug Des.* **2014**, *83*, 306–316; c) S. Tomassi, J. Lategahn, J. Engel, M. Keul, H. L. Tumbrink, J. Ketzer, T. Mühlenberg, M. Baumann, C. Schultz-Fademrecht, S. Bauer, D. Rauh, *J. Med. Chem.* **2017**, *60*, 2361–2372.
[9] P. Nareddy, F. Jordan, M. Szostak, *ACS Catal.* **2017**, *7*, 5721–5745.
[10] J. J. Song, N. K. Yee, *Org. Lett.* **2000**, *2*, 519–522.
[11] a) N. Halland, M. Nazaré, O. R'kyek, J. Alonso, M. Urmann, A. Lindenschmidt, *Angew. Chem. Int. Ed.* **2009**, *48*, 6879–6885; *Angew. Chem.* **2009**, *121*, 7011–7014; b) C. Wu, Y. Fang, R. C. Larock, F. Shi, *Org. Lett.* **2010**, *12*, 2234–2237; c) B. J. Stokes, C. V. Vogel, L. K. Urnezis, M. Pan, T. G. Driver, *Org. Lett.* **2010**, *12*, 2884–2887; d) B. Haag, Z. Peng, P. Knochel, *Org. Lett.* **2009**, *11*, 4270–4273; e) Y. Lian, R. G. Bergman, L. D. Lavis, J. A. Ellman, *J. Am. Chem. Soc.* **2013**, *135*, 7122–7125; f) N. E. Genung, L. Wei, G. E. Aspnes, *Org. Lett.* **2014**, *16*, 3114–3117; g) Z. Long, Y. Yang, J. You, *Org. Lett.* **2017**, *19*, 2781–2784; h) Z. Long, Z. Wang, D. Zhou, D. Wan, J. You, *Org. Lett.* **2017**, *19*, 2777–2780.
[12] M. R. Kumar, A. Park, M. Park, S. Lee, *Org. Lett.* **2011**, *13*, 3542–3545.
[13] H. Sharghi, M. Aberi, *Synlett* **2014**, *25*, 1111–1115.
[14] a) I. Lee, F. Delbecq, R. Morales, M. A. Albiter, F. Zaera, *Nat. Mater.* **2009**, *8*, 132–138; b) Y. Wu, S. Cai, D. Wang, W. He, Y. Li, *J. Am. Chem. Soc.* **2012**, *134*, 8975–8981.
[15] a) M. Li, X. Xing, Z. Ma, J. Lv, P. Fu, Z. Li, *ACS Sustainable Chem. Eng.* **2018**, *6*, 5495–5503; b) C.-S. Tan, S.-C. Hsu, W.-H. Ke, L.-J. Chen, M. H. Huang, *Nano Lett.* **2015**, *15*, 2155–2160; c) Y. Su, H. Li, H. Ma, J. Robertson, A. Nathan, *ACS Appl. Mater. Interfaces* **2017**, *9*, 8100–8106.
[16] a) K. Chanda, S. Rej, M. H. Huang, *Chem. Eur. J.* **2013**, *19*, 16036–16043; b) K. Chanda, S. Rej, M. H. Huang, *Nanoscale* **2013**, *5*, 12494–12501; c) Y.-H. Tsai, K. Chanda, Y.-T. Chu, C.-Y. Chiu, M. H. Huang, *Nanoscale* **2014**, *6*, 8704–8709.

[17] S. Rej, K. Chanda, C.-Y. Chiu, M. H. Huang, *Chem. Eur. J.* **2014**, *20*, 15991–15997.

[18] a) B. Maiti, K. Chanda, *RSC Adv.* **2016**, *6*, 50384–50413; b) R. N. Rao, B. Maiti, K. Chanda, *ACS Comb. Sci.* **2017**, *19*, 199–228; c) R. N. Rao, M. M. Balamurali, B. Maiti, R. Thakuria, K. Chanda, *ACS. Comb. Sci.* **2018**, *20*, 164–171; d) R. D. Padmaja, K. Chanda, *Org. Process Res. Dev.* **2018**, *22*, 457–466; e) R. D. Padmaja, C. V. Devi, N. Mukku, K. Chanda, B. Maiti, *ACS Omega* **2018**, *3*, 4583–4590.

[19] a) R. A. Sheldon, *Green Chem.* **2007**, *9*, 1273–1283; b) R. A. Sheldon, *Chem. Soc. Rev.* **2012**, *41*, 1437–1451.

[20] a) C. A. Lipinski, F. Lombardo, B. W. Dominy, P. J. Feeney, *Adv. Drug Delivery Rev.* **1997**, *23*, 3–25; b) C. A. Lipinski, F. Lombardo, B. W. Dominy, P. J. Feeney, *Adv. Drug Delivery Rev.* **2001**, *46*, 3–26; c) D. F. Veber, S. R. Johnson, H.-Y. Cheng, B. R. Smith, K. W. Ward, K. D. Kopple, *J. Med. Chem.* **2002**, *45*, 2615–2623.

[21] H. E. B. Lempers, R. A. Sheldon, *J. Catal.* **1998**, *175*, 62–69.

[22] N. M. Y. Elsayed, D. A. Abou El Ella, R. A. T. Serya, M. F. Tolba, R. Shalaby, K. A. M. Abouzid, *Med. Chem. Commun.* **2016**, *7*, 881–899.

[23] S. Horibata, T. V. Vo, V. Subramanian, P. R. Thompson, S. A. Coonrod, *J. Vis. Exp.* **2015**, e52727.

[24] J. M. Brown, L. D. Attardi, *Nat. Rev. Cancer* **2005**, *5*, 231–237.

[25] S. Sakamuru, M. S. Attene-Ramos, M. Xia in *High-Throughput Screening Assays in Toxicology. Methods in Molecular Biology Vol. 1473* (Eds.: H. Zhu, M. Xia), Humana Press, New York, **2016**, pp. 17–22.

[26] M. L. Coleman, E. A. Sahai, M. Yeo, M. Bosch, A. Dewar, M. F. Olson, *Nat. Cell Biol.* **2001**, *3*, 339–345.

[27] Y. Zhang, X. Chen, C. Gueydan, J. Han, *Cell Res.* **2018**, *28*, 9–21.

[28] Y. Shi, *Protein Sci.* **2004**, *13*, 1979–1987.

[29] R. Riahi, Y. Yang, D. D. Zhang, P. K. Wong, *J. Lab. Autom.* **2012**, *17*, 59–65.

[30] D. Hanahan, R. A. Weinberg, *Cell* **2011**, *144*, 646–674.

[31] T. Mosmann, *J. Immunol. Methods* **1983**, *65*, 55–63.

[32] S. Anjana, J. E. Thoppil, *Int. J. Res. Dev. Pharm. L. Sci.* **2013**, *2*, 562–566.

[33] D. Gao, H. Hu, Y. Wang, W. Yu, J. Zhou, X. Wang, W. Wang, C. Zhou, K. Xu, *Oncol. Rep.* **2015**, *34*, 2853–2863.

[34] L. Liu, J. Zhang, M. Li, X. Zhang, J. Zhang, Z. Li, L. Wang, J. Wu, C. Luo, *Mol. Med. Rep.* **2014**, *9*, 2505–2511.

[35] L. Kastl, S. W. Sauer, T. Ruppert, T. Beissbarth, M. S. Becker, D. Suss, *FEBS Lett.* **2014**, *588*, 175–183.

[36] N. Cormier, A. Yeo, E. Fiorentino, J. Paxson, *J. Vis. Exp.* **2015**, *106*, e53414.